2020 IEEE/RSJ International Conference on Intelligent Robots and Systems (IROS)
October 25-29, 2020, Las Vegas, NV, USA (Virtual)

Design and implementation of a pipeline inspection robot with camera image compensation

Zhaohan Yuan, Jianjun Yuan*, *Member, IEEE*, Shugen Ma, *IEEE Fellow*

***Abstract*— In this paper, we updated an inspection robot with passive adaptation ability, which is used to detect small size water supply pipeline. By geometric calculation and kinematic verification, static model of the robot is checked for flexible movement in the pipeline. Besides, inertial measurement unit is leveraged to simultaneously detect the attitude of robot, and different algorithm is tested to compensate the camera image rotation, stabilizing the image output.**

I. Introduction

The urban water supply and drainage network are the "blood of the city". With the continuous development and expansion of the water supply and drainage network in China, its problems continue to emerge. Damage to old pipes has caused problems such as sewage overflow, water pollution, and road subsidence, damaging both environment and property. Therefore, repairing, detection and prevention of water supply and drainage pipelines are of great significance for maintaining urban order. With low effectiveness of traditional excavation, non-excavation repair techniques are preferred in recent decades, and robots with strong dynamic performance are commonly used to test pipeline, carrying relevant sensor for condition detection.

From 1980s, different types of pipeline robots have been researched. Hirose, Ohno developed wheeled robots Theseus-I Theseus-II and Theseus-III for pipes inspection. Elastic rods are used to press the inner walls of the pipeline, powered by batteries and brushless motors to drive the wheels. The maximum walking distance exceeds 150m [1]. Hun-ok Lim designed a wheeled pipeline robot, whose legs are evenly distributed at 120 ° to offer enough tension and accommodate different pipe sizes, carrying CCD camera [2]. Se-gon Roh developed MRINSPECT IV wheeled pipeline robot for gas pipeline inspection, whose drive module is connected by spring, being able to expanded or contracted to accommodate different pipe sizes [3]. Minoru Kurata proposed a helical rotating pipe robot, which is fixed on the body axis at a certain angle by wires. When these wires are contracted and extended once, the body as a whole will rotate and move forward without slipping [4].

To provide tension, most pipeline robots extrude the inner wall of pipeline symmetrically, with less flexibility to adapt complex pipeline, such as arc and 'L' shape pipeline. In 2016, team of Shugen Ma developed a multilink-articulated wheeled pipeline inspection robot with passive elastic joints, which had strong adaptability to small pipeline [5-7]. However, its rotation capability is not stable during curving pipeline crawling, and pipeline inspection feedback data is limited. In this paper, we update the pipeline inspection robot, with below differentiations and innovations: 1) revised mechanical body and torsion spring, to adapt pipeline inclusively, 2) updated rolling system to pass curved pipeline effectively, 3) design camera compensation system to stabilize image output.

The rest of this paper is organized as follows. In section II, robot attitude and static force are analyzed. In section III, camera image compensation is described and tested. Finally, section IV concludes the paper.

Zhaohan Yuan is with the Robotics Institute of Shanghai Jiao Tong University, 800 Dongchuan RD, Minhang District, Shanghai (e-mail: yzh19950725@ sjtu.edu.cn).

Jianjun Yuan is with Shanghai Robotics Institute, Shanghai Key Laboratory of Intelligent Manufacturing and Robotics, School of Mechatronic Engineering and Automation, Shanghai University (corresponding author, phone: +86-21-66132128, e-mail: terabit@shu.edu.cn).

Shugen Ma is with the Department of Robotics, Ritsumeikan University, Shiga, Japan. (e-mail: shugen.ma@ieee.org)

II. Attitude and Static Analysis

A. Pipeline Constraint and Attitude Calculation

Pipeline robot consists of four joints, connecting as 'M' shape. Fig.1 shows the attitude of the robot. $L_i(i=1-4)$ are the length of joints, and $p_i(i=1-5)$ are the centers of the wheels. All wheels in $p_i(i=1-5)$ are equipped with driving motors, while p_1 and p_5 provides rotation torque to adjust roll angle of the robot, paralleling the planes of 'M' and curved pipeline to pass the bending, and p_2, p_3 and p_4 act as driving wheels. To satisfy both driving forward and roll axis rotation, all five wheels are Omni wheels, providing one more DOF. The basic parameters of robot and pipeline are shown as TABEL I and TABEL II. To make specific calculation and experiment, pipeline diameter is taken as 0.15m in this paper.

Different from flat land, robot with wheel in pipeline has more constraint, which is shown as Fig.2(a). Diameter of pipeline, width of robot and radius of wheels all constrain the attitude of robot. According to geometry of circle, vertical distance between driving wheels is:

$$H=\sqrt{D^2-W^2} \tag{1}$$

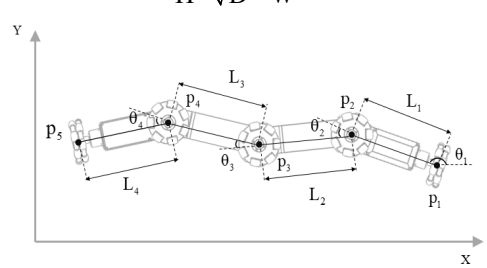

Figure 1. Kinematic parameters of inspection robot

TABLE I. PARAMESTERS OF ROBOT

Mass of joint 1 (m1) (kg)	1.1
Mass of joint 2 (m2) (kg)	1.29
Mass of joint 3 (m3) (kg)	1.05
Mass of joint 4 (m4) (kg)	0.97
Length of joint (L_i , i=1,4) (m)	0.185
Length of joint (L_i , i=2,3) (m)	0.18
Width of robot (W) (m)	0.103
Radius of rotation wheel (R1) (m)	0.04
Radius of driving wheel (R2) (m)	0.04

TABLE II. PARAMETERS OF PIPELINE

Diameter of pipeline (D) (m)	0.12-0.18
Radius of pipeline (R_b) (m)	0.13
Static friction coefficient between wheels and wall (μ)	0.4
Roll friction coefficient between wheels and wall (μ_R)	0.05

Vertical distance between inner wall and the driving wheel is:

$$\Delta \mathrm{H}=\frac{1}{2}(\mathrm{D}\text{-}\mathrm{H}) \tag{2}$$

In pipeline movement, the angles between each joint verify with pipeline inner situation, shown as Fig.2 (b).
By geometric restriction:

$$\theta_1=\pi-\beta_1+\alpha_1 \tag{3}$$

$$\theta_2=\pi-\beta_2+\alpha_2-\theta_1 \tag{4}$$

$$\theta_3=\pi-\beta_3+\alpha_3-\theta_1-\theta_2 \tag{5}$$

$$\theta_4=\pi-\beta_4+\alpha_4-\theta_1-\theta_2-\theta_3 \tag{6}$$

where

$$\beta_i=\cos^{-1}\frac{l_{i-1}^{\ 2}+L_i^{\ 2}-l_i^2}{2l_{i-1}L_i}(i=1,2,3,4)$$

$$\alpha_i=\tan^{-1}\frac{y_{i-1}}{x_{i-1}}(i=1,2,3,4)$$

And l_i is the distance between driving wheels and geometrical center of curved pipeline:

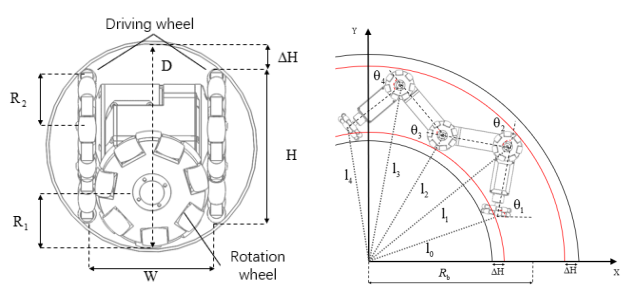

(a) (b)

Figure 2. Geometric restriction of inspection robot

$$l_i=\begin{cases} R_b-\dfrac{D}{2}+R_1\,(i=0,4) \\ R_b+\dfrac{D}{2}-\Delta\mathrm{H}-R_2\,(i=1,3) \\ R_b-\dfrac{D}{2}+\Delta\mathrm{H}+R_2\,(i=2) \end{cases} \tag{7}$$

When robot is moving in the straight pipeline, R_b is infinite, and formula is simplified as:

$$\theta_1=\cos^{-1}\frac{D-\Delta\mathrm{H}-R_1-R_2}{L_1} \tag{8}$$

$$\theta_2=\cos^{-1}\frac{-(D-2\Delta\mathrm{H}-2R_2)}{L_2}-\theta_1 \tag{9}$$

$$\theta_3=\cos^{-1}\frac{D-2\Delta\mathrm{H}-2R_2}{L_3}-\theta_1-\theta_2 \tag{10}$$

$$\theta_4=\cos^{-1}\frac{-(D-\Delta\mathrm{H}-R_1-R_2)}{L_4}-\theta_1-\theta_2-\theta_3 \tag{11}$$

Based on robot and pipeline parameters in TABLE I and TABLE II, the attitude angles of each in straight pipeline are θ_1=74.5° , θ_2=24.8° , $\theta_3=-18.6°$, θ_4=24.8° . The attitude angles will change in a small range when pipeline diameter changes.

B. Static Model Verification

In the pipeline, the greater the torque produced by the torsion spring, the greater the positive pressure and corresponding maximum static friction on the wheels. However, due to the limitation of the internal space of the robot, the torsion spring parameters are supposed to be tested. The verification standards of torsion springs in the robot are as follows: 1) Provide enough torque to avoid slipping of driving wheels, 2) The size adapts to internal structure of the robot with tight fit, 3) Reduce the elasticity as much as possible to avoid cornering.

Combined with the robot's internal structure and processing material restrictions, piano wire is preliminarily chosen. The wire diameter is 3.5mm, and the spring diameter can be selected from 24-28mm, while the number of turns can be between 5 and 7.

As vertical straight motion and vertical curvilinear motion are two typical movements with universality, in the following of this chapter, we analyze these two motions to rationally choose the specific parameters of torsion spring and verify static model of robot.

When moving vertically upward in the pipeline, the robot is subjected to gravity, pressure, rolling friction, and torque generated by the torsion spring deformation, as shown in the Fig.3, where $N_i(i=0-4)$ is the positive pressure of the pipeline on the robot, $f_i(i=0-4)$ is the friction received by the wheels, G is the gravity, and $\tau_i(i=1-3)$ is the torque provided by the torsion spring.

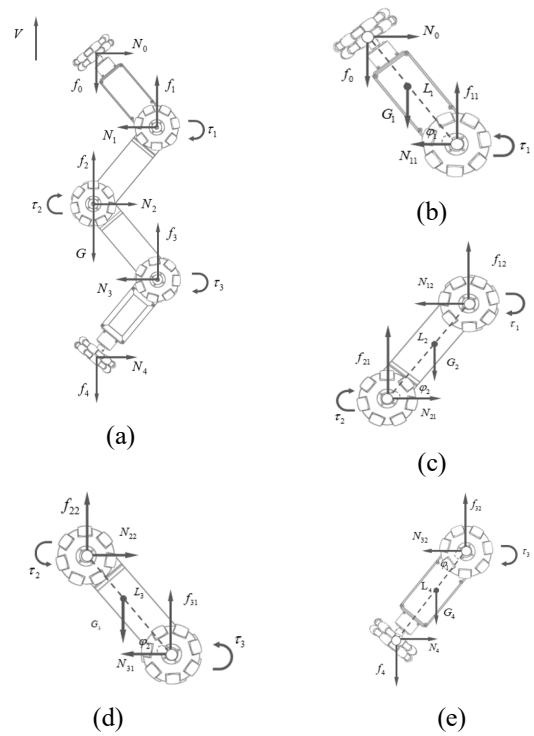

Figure 3. Static model of robot in vertically upward movement (a) whold robot, (b-e) four joints of robot

With equilibrium of force for each joint:

$$\begin{bmatrix} \mathbf{N_u} - \mathbf{N_d} \\ \mathbf{f_u} - \mathbf{f_d} \end{bmatrix} = \begin{bmatrix} \mathbf{O} \\ \mathbf{G} \end{bmatrix} \tag{12}$$

where

$$\mathbf{N_u} = \begin{bmatrix} N_0 & N_{12} & N_{22} & N_{32} \end{bmatrix}^{\mathrm{T}}$$

$$\mathbf{N_d} = \begin{bmatrix} N_{11} & N_{21} & N_{31} & N_4 \end{bmatrix}^{\mathrm{T}}$$

$$\mathbf{G} = \begin{bmatrix} G_1 & G_2 & G_3 & G_4 \end{bmatrix}^{\mathrm{T}}$$

$$\mathbf{f_u} = \begin{bmatrix} -\mathrm{f}_0 & \mathrm{f}_{12} & \mathrm{f}_{22} & \mathrm{f}_{32} \end{bmatrix}^{\mathrm{T}}$$

$$\mathbf{f_d} = \begin{bmatrix} \mathrm{f}_{11} & \mathrm{f}_{21} & \mathrm{f}_{31} & -\mathrm{f}_4 \end{bmatrix}^{\mathrm{T}}$$

where $f_{ij}\left(i, j = 0-4\right)$ is friction and $N_{ij}\left(i, j = 0-4\right)$ is wall supporting force.

With equilibrium of moment for each joint:

$$\boldsymbol{\tau} + \frac{1}{2}\mathrm{diag}\left(\mathbf{G}\right)\mathbf{L_c} = \mathrm{diag}\left(\mathbf{N_u}\right)\mathbf{L_s} + \mathrm{diag}\left(\mathbf{f_u}\right)\mathbf{L_c} \tag{13}$$

where

$$\boldsymbol{\tau} = \begin{bmatrix} \tau_1 & \tau_1 + \tau_2 & \tau_2 + \tau_3 & \tau_3 \end{bmatrix}^{\mathrm{T}}$$

$$\mathbf{L_c} = \begin{bmatrix} L_1 \cos\varphi_1 & L_2 \cos\varphi_2 & L_3 \cos\varphi_3 & L_4 \cos\varphi_4 \end{bmatrix}^{\mathrm{T}}$$

$$\mathbf{L_s} = \begin{bmatrix} L_1 \sin\varphi_1 & L_2 \sin\varphi_2 & L_3 \sin\varphi_3 & L_4 \sin\varphi_4 \end{bmatrix}^{\mathrm{T}}$$

In the formula, $f_i(i = 0,4)$ is the rolling friction, so $f_i = \mu_R N_i (i = 0-4)$, where μ_R is coefficient of rolling friction. And assumption is made that driving force of each motor is the same, shown as $f_{11} + f_{12} = f_{21} + f_{22} = f_{31} + f_{32}$.

The driving force is supposed to not exceed the maximum of static friction, to prevent slipping of driving wheels.

$$f_i \le \mu N_i (i = 1,2,3) \tag{14}$$

where μ if coefficient of maximum static friction.

With specific parameters of robot, Fig.4 and Fig.5 show the static verification of robot in vertical straight movement. By Fig.4, the driving force is not greatly affected by the diameter and turn of the torsion spring, and basically forms a plane, which is approximately equal to maximum static friction force. When the diameter and turns of the torsion spring are gradually reduced, wheel 3 will be the first to slip. To independently analyze the wheel 3, XY projection is made, shown as Fig.5. The dashed line is the boundary, over which the driving wheel is supposed to slip.

Base on above analysis and constrain of internal structure, torsion spring with diameter 28mm and turns 6 is chosen for analysis in next part.

Then, vertical curvilinear motion is another typical motion in pipeline inspection, whose statics model of curvilinear motion is similar to last character, shown as Fig.6.

The equilibriums of force and moment for each joint are applied as follow:

$$\mathrm{diag}\left(\mathbf{f_u}\right)\mathbf{c}_{\alpha 1} + \mathrm{diag}\left(\mathbf{f_d}\right)\mathbf{c}_{\alpha 0} + \mathrm{diag}\left(\mathbf{AN_u}\right)\mathbf{s}_{\alpha 1} - \mathrm{diag}\left(\mathbf{AN_d}\right)\mathbf{s}_{\alpha 0} = \mathbf{G} \tag{15}$$

$$\mathrm{diag}\left(\mathbf{f_u}\right)\mathbf{s}_{\alpha 1} + \mathrm{diag}\left(\mathbf{f_d}\right)\mathbf{s}_{\alpha 0} - \mathrm{diag}\left(\mathbf{AN_u}\right)\mathbf{c}_{\alpha 1} + \mathrm{diag}\left(\mathbf{AN_d}\right)\mathbf{c}_{\alpha 0} = \mathbf{0} \tag{16}$$

$$\mathrm{diag}\left(\mathbf{f_u}\right)\mathbf{l_0} + \mathrm{diag}\left(\mathbf{f_d}\right)\mathbf{l_1} - \mathrm{diag}\left(\mathbf{G}\right)\left(\mathbf{l_0}\mathbf{c}_{\alpha 0} + \frac{1}{2}\mathbf{L}\mathbf{c_0}\right) = \mathbf{0} \tag{17}$$

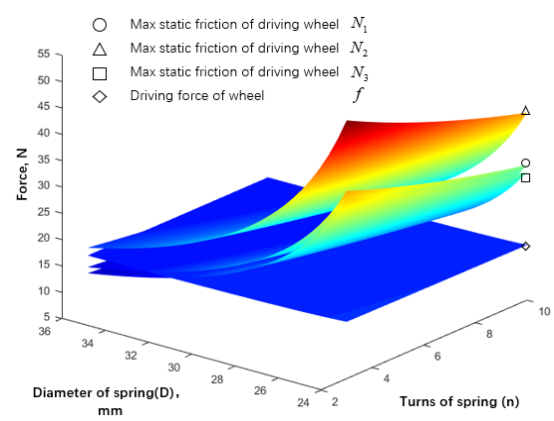

Figure 4. Static verification in vertically upward movement

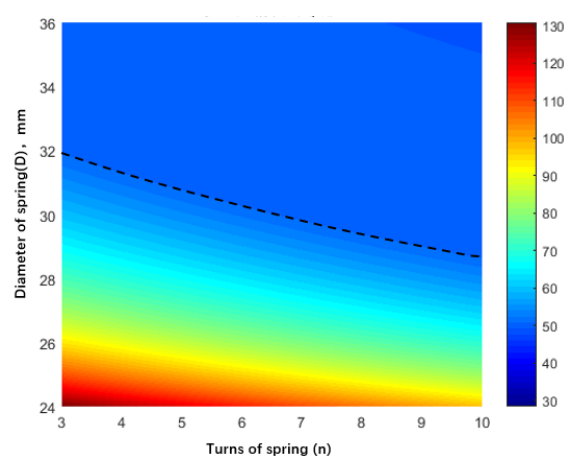

Figure 5. Projection of wheel 3 friction and driving force

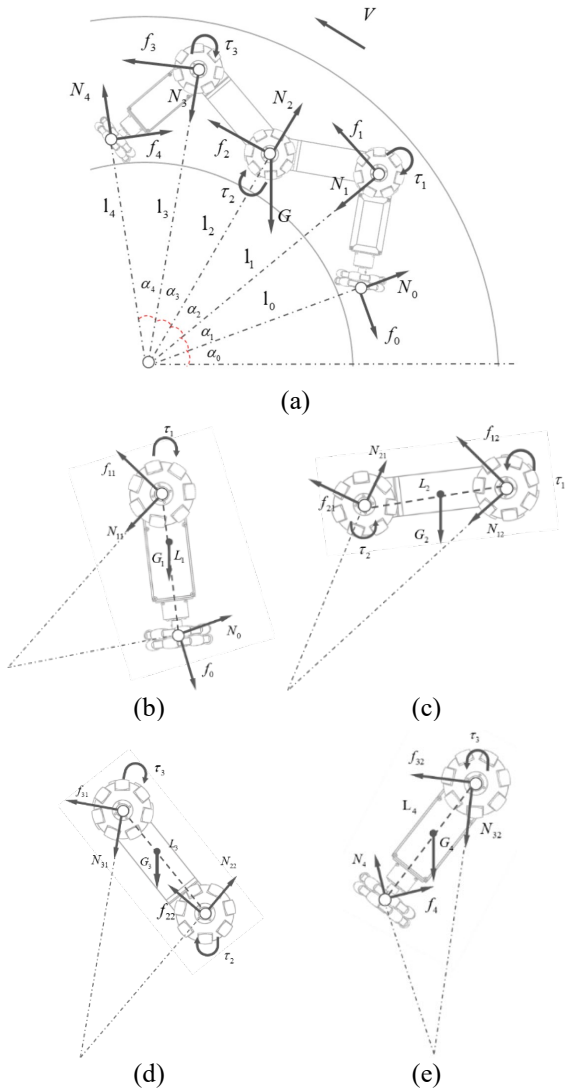

Figure 6. Static model of robot in vertically curvilinear movement (a) whold robot, (b-e) four joints of robot

where

$$\mathbf{c}_{\alpha 0}=\begin{bmatrix}\cos\alpha_0 & \cos\alpha_{0-1} & \cos\alpha_{0-2} & \cos\alpha_{0-3}\end{bmatrix}^{\mathrm{T}}$$

$$\mathbf{c}_{\alpha 1}=\begin{bmatrix}\cos\alpha_{0\text{-}1} & \cos\alpha_{0\text{-}2} & \cos\alpha_{0\text{-}3} & \cos\alpha_{0\text{-}4}\end{bmatrix}^{\mathrm{T}}$$

$$\mathbf{s}_{\alpha 0}=\begin{bmatrix}\sin\alpha_0 & \sin\alpha_{0-1} & \sin\alpha_{0-2} & \sin\alpha_{0-3}\end{bmatrix}^{\mathrm{T}}$$

$$\mathbf{s}_{\alpha 1}=\begin{bmatrix}\sin\alpha_{0\text{-}1} & \sin\alpha_{0\text{-}2} & \sin\alpha_{0\text{-}3} & \sin\alpha_{0\text{-}4}\end{bmatrix}^{\mathrm{T}}$$

$$\mathbf{c}_{\theta}=\begin{bmatrix}\cos\theta_1 & \cos\theta_{1\text{-}2} & \cos\theta_{1\text{-}3} & \cos\theta_{1\text{-}4}\end{bmatrix}^{\mathrm{T}}$$

$$A=diag(\begin{bmatrix}1 & -1 & 1 & -1\end{bmatrix}^{\mathrm{T}}),\ \mathbf{l}_0=\begin{bmatrix}l_0 & l_1 & l_2 & l_3\end{bmatrix}^{\mathrm{T}}$$

$$\mathbf{l}_1=\begin{bmatrix}l_1 & l_2 & l_3 & l_4\end{bmatrix}^{\mathrm{T}},\ \mathbf{L}=\begin{bmatrix}L_1 & L_2 & L_3 & L_4\end{bmatrix}^{\mathrm{T}}$$

in which $\alpha_{0-i}=\alpha_0+\cdots+\alpha_i(i=1-4)$ and $\theta_{1-i}=\theta_1+\cdots+\theta_i(i=2-4)$.

In the formula, $f_i(i=0,4)$ is the rolling friction, so $f_i=\mu_R N_{\mathrm{i}}(i=0,4)$, where μ_R is coefficient of rolling friction.

And assumption is made that driving force of each motor is the same, applying as $f_{11}+f_{12}=f_{21}+f_{22}=f_{31}+f_{32}$.

The driving force is supposed to not exceed the maximum of static friction, to prevent slipping of driving wheels, so:

$$f_i \le \mu N_{\mathrm{i}}\ (\mathrm{i}=1,2,3) \tag{18}$$

where μ if coefficient of maximum static friction.

Fig.7 and Fig.8 show the static verification of robot in vertical curvilinear motion. The driving force varies with the initial angle, and it changes periodically in a sinusoidal form. When $k=0.05Nm/Deg$, the driving force is always less than the maximum static friction of each wheel, meaning that no slipping will occur. Therefore, in this project, coefficient of spring is taken as 0.05Nm/Deg.

III. Camera Image Compensation

When the pipeline robot moves in the pipeline, it is restricted by its M-shaped structure and the inner wall of the pipeline. The pitch and yaw angles of the pipeline robot will not change. However, because the direction of the pipeline curve is unknown, the robot needs to drive rolling wheels to change its roll angle so that the plane where the M-shaped structure is located is parallel to the plane formed by the pipe curve. It means that during the movement, the robot's roll angle always changes, which in turn causes the pipeline image output by the camera to be constantly rotating, making it difficult for workers to determine specific inner situation, such as damage and scars in the pipeline. Therefore, the camera output is supposed to be stable, which is of great importance for pipeline robots.

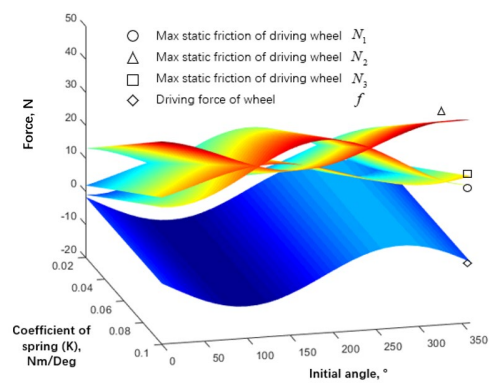

Figure 7. Static verification in vertically curvilinear movement

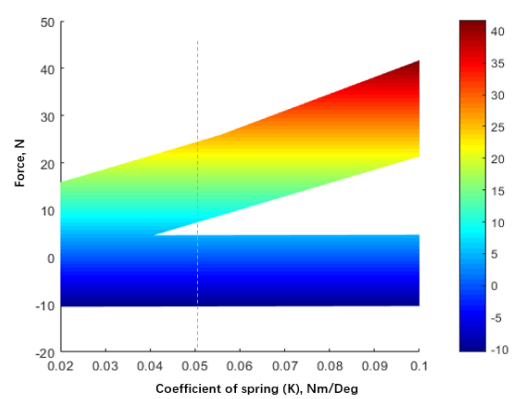

Figure 8. Projection of spring coefficient and relative force

Image stabilization can be achieved by two methods: image processing stabilization and structural compensation stabilization. Image processing stabilization requires the camera to output the image in real time, and identify feature points with algorithms, then determine image rotation information to make compensation. However, its shortcomings are: 1) the image in the pipeline returned by the camera has fewer recognizable feature points, and the image recognition process is difficult; 2) the real-time processing of image recognition and rotation requires high back-end processing capabilities. In order to reduce the background processing burden and achieve stable and efficient image stability, the pipeline robot adopts a front-end structure compensation method, by rotating the camera with a compensation angle.

A. Compensation Design

In order to measure the change of the roll angle of the pipeline robot in real time, inertial measurement unit (IMU) is used to measure camera-related motion trajectories to achieve image stability. The IMU is usually equipped with a three-axis accelerometer and a three-axis gyroscope, which are installed on the measured object and widely used in diversify industries [8-11], can effectively measure the acceleration and angular velocity of the object, and then calculate the attitude angle.

In this project, SparkFun 9DoF Razor IMU M0 is installed inside the first link of robot to test the roll angle, containing a micro-processor and an MPU-9250 sensor. All accelerometer, gyroscope and magnetic sensor are included. Then an endoscopy is used as image sensor, installed on the first link, and a digital servo motor is leveraged to rotate the camera. And the whole process is shown as Fig.10

B. Compensation Result

The compensation system needs to read the rotation angle of the robot in real time, and output the compensation angles with the same speed and opposite directions through the servo motor in real time. To achieve this goal, the servo motor can be controlled in two ways: speed control or speed & position control.

Due to the special nature of the servo, there is a potentiometer inside it to achieve simple closed-loop control.

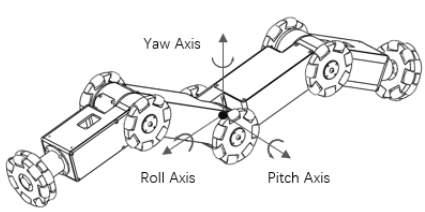

Figure 9. Attitude of inspection robot

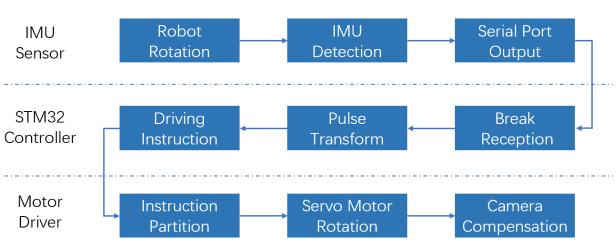

Figure 10. Camera image compensation process

With simple speed control, a certain error between the actual angular speed and the theoretical angular speed at the peak and valley values accumulated. With increasing of movement time, this error keeps accumulating, which causes the error of the compensation continue to enlarge, making it difficult to maintain the stability of image output.

To eliminate cumulative error, this project uses a speed & position control method, detecting both speed and angle position of the robot, to improve the stability of the image. In this method, real time speed is detected directly by angular sensor of IMU, and rolling position is also available by quaternion transformation or angular velocity integration.

With accelerometer and magnetic sensor in IMU, the Euler angle of the robot is derived as:

$$Roll = \arctan\left(\frac{a_y}{a_z}\right) \tag{19}$$

$$Pitch = -\arctan\left(\frac{a_x}{\sqrt{a_y^2 + a_z^2}}\right) \tag{20}$$

$$Yaw = \arctan\left(\frac{m_z s_R - m_y c_R}{m_x c_P + m_y s_R s_P + m_z c_R s_P}\right) \tag{21}$$

where $a_i (i = x, y, z)$ is the acceleration, $m_i (i = x, y, z)$ is the magnetic field data. To avoid risk of deadlock, Euler angle is transferred to quaternion in the following algorithm [12].

With restricts of movement in other dimensions, and only periodically rolling the robot around x axis, the roll angle recognition effect is shown in Fig.11 below. In this simple motion state, the quaternion transformation algorithm and the angular velocity integration method have basically the same effect. The maximum errors are 8.6 ° and 8.9 ° respectively.

In real inspection process, the movement is more complicated. To simulate real moving situation, restriction of other dimensions is eliminated, and pitch and yaw of the robot are irregularly changed while the roll angle is rotating periodically. The roll angle recognition result is shown in the Fig.12 below. It shows that with interference from the other directions, the quaternion transformation algorithm performs significantly better than the angular velocity integration method. The former has a maximum error of 29.9 °and a relative error of approximately 16.6%, while the latter has an

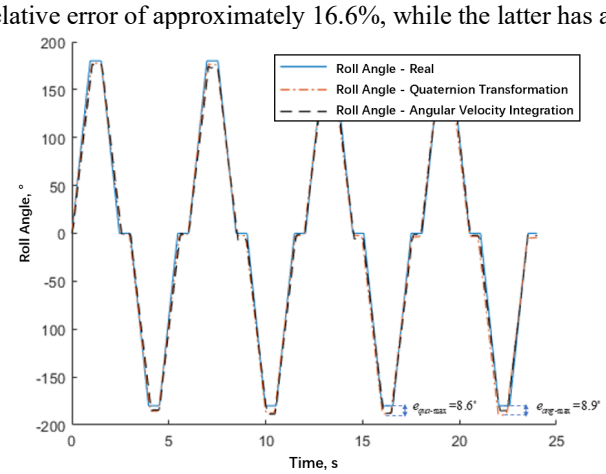

Figure 11. Roll angle compensation comparision without interrupt

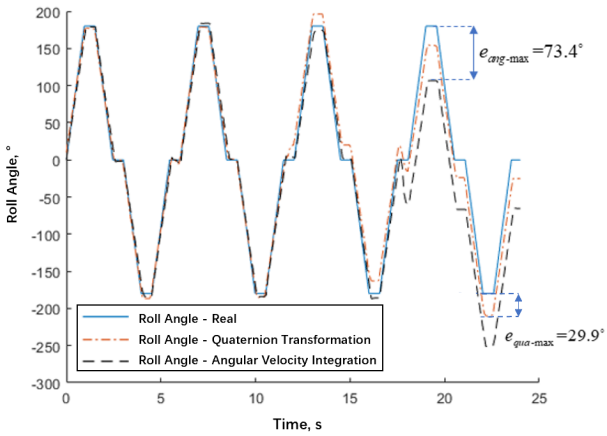

Figure 12. Roll angle compensation comparision with interrupt

absolute maximum error of 73.4 ° and a relative error of 40.8%, for the reason that angular velocity is susceptible to interference and a large number of abnormal values are caused and accumulated.

In order to maintain the stability of the camera and reduce the angle error, we modified the quaternion transformation by identifying and revising abnormal data with filter [13]. After revision, the roll angle compensation result is shown as Fig.13, and maximum error is reduced to 11.9 °, with relative error of 6.6%.

The rotation compensation results are shown as Fig.14 and Fig.15. With above compensation algorithm, the output camera images are stable without rotation

IV. Conclusion

In this paper, we updated an inspection robot with passive adaptation ability, which is used to detect small size water supply pipeline. With attitude calculation and static verification, the statics model of the robot is checked for stable movement in the pipeline. Besides, IMU is leveraged to simultaneously test the attitude of robot, and different algorithm is tested to compensate the camera image rotation, stabilizing the image output.

In next step, IMU is expected to be further leveraged to visualized pipeline model by simulation, which will help inspecting staff to better understand pipeline situation. The relative simulation and experiment are in the process.

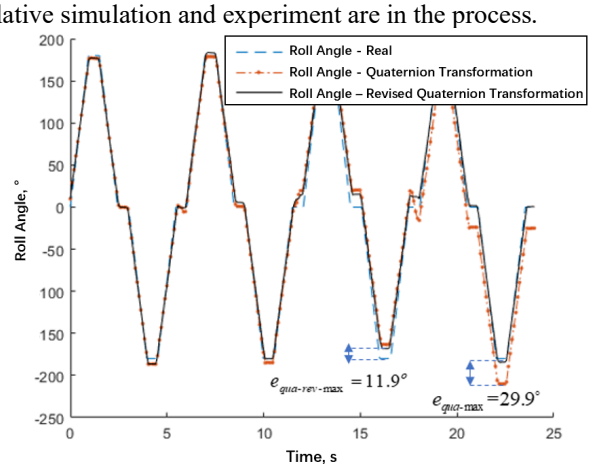

Figure 13. Roll angle compensation with revised algorithm

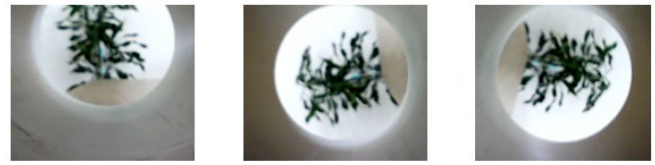

(a) (b) (c)

Figure 14. Camera image without rotation compensation

(a) (b) (c)

Figure 15. Camera image with rotation compensation

References

[1] S. Hirose, H. Ohno, T. Mitsui and K. Suyama, "Design of in-pipe inspection vehicles for 25, 50, 150 pipes," Proceedings 1999 IEEE International Conference on Robotics and Automation, 1999, pp. 2309-2314 vol.3.

[2] L. Hun-ok and O. Taku, "Development of pipe inspection robot," 2009 ICCAS-SICE, Fukuoka, 2009, pp. 5717-5721.

[3] R. Se-gon and C. Hyouk Ryeol, "Differential-drive in-pipe robot for moving inside urban gas pipelines," in IEEE Transactions on Robotics, vol. 21, no. 1, pp. 1-17, Feb. 2005.

[4] M. Kurata, T. Takayama and T. Omata, "Helical rotation in-pipe mobile robot," 2010 3rd IEEE RAS & EMBS International Conference on Biomedical Robotics and Biomechatronics, Tokyo, 2010, pp. 313-318.

[5] A. Kakogawa and S. Ma, "Design of a multilink-articulated wheeled inspection robot for winding pipelines: AIRo-II," 2016 IEEE/RSJ International Conference on Intelligent Robots and Systems (IROS), Daejeon, 2016, pp. 2115-2121.

[6] A. Kakogawa, Y. Oka and S. Ma, "Multi-link Articulated Wheeled In-pipe Robot with Underactuated Twisting Joints," 2018 IEEE International Conference on Mechatronics and Automation (ICMA), Changchun, 2018, pp. 942-947.

[7] A. Kakogawa, Y. Komurasaki and S. Ma, "Anisotropic shadow-based operation assistant for a pipeline-inspection robot using a single illuminator and camera," 2017 IEEE/RSJ International Conference on Intelligent Robots and Systems (IROS), Vancouver, BC, 2017, pp. 1305-1310.

[8] S. Sukkarieh, E. M. Nebot and H. F. Durrant-Whyte, "A high integrity IMU/GPS navigation loop for autonomous land vehicle applications," in IEEE Transactions on Robotics and Automation, vol. 15, no. 3, pp. 572-578, June 1999.

[9] S. O. H. Madgwick, A. J. L. Harrison and R. Vaidyanathan, "Estimation of IMU and MARG orientation using a gradient descent algorithm," 2011 IEEE International Conference on Rehabilitation Robotics, Zurich, 2011, pp. 1-7.

[10] A. R. Jimenez Ruiz, F. Seco Granja, J. C. Prieto Honorato and J. I. Guevara Rosas, "Accurate Pedestrian Indoor Navigation by Tightly Coupling Foot-Mounted IMU and RFID Measurements," in IEEE Transactions on Instrumentation and Measurement, vol. 61, no. 1, pp. 178-189, Jan. 2012.

[11] F. M. Mirzaei and S. I. Roumeliotis, "A Kalman Filter-Based Algorithm for IMU-Camera Calibration: Observability Analysis and Performance Evaluation," in IEEE Transactions on Robotics, vol. 24, no. 5, pp. 1143-1156, Oct. 2008.

[12] M. D. Henderson, "Euler angles, quaternions, and transformation matrices for space shuttle analysis." ,1977.

[13] S. M. Seong, J. G. Lee, C. G. Park, "Equivalent ARMA model representation for RLG random errors". IEEE transactions on aerospace and electronic systems, 2000, 36(1): 286-290.